

SweetTokenizer: Semantic-Aware Spatial-Temporal Tokenizer for Compact Visual Discretization

Zhentao Tan*, Ben Xue*, Jian Jia, Junhao Wang, Wencai Ye, Shaoyun Shi, Mingjie Sun
Wenjin Wu, Quan Chen†, Peng Jiang
Kuaishou Technology, Beijing, China

{tanzhentao03, xueben, jiajian, wangjunhao05, yewencai, shishaoyun,
sunmingjie, wuwenjin, chenquan06, jiangpeng}@kuaishou.com

Abstract

This paper presents the *Semantic-aWare spatial-tEmporal Tokenizer* (*SweetTokenizer*), a compact yet effective discretization approach for vision data. Our goal is to boost tokenizers’ compression ratio while maintaining reconstruction fidelity in the VQ-VAE paradigm. Firstly, to obtain compact latent representations, we decouple images or videos into spatial-temporal dimensions, translating visual information into learnable querying spatial and temporal tokens through a Cross-attention *Query AutoEncoder* (CQAE). Secondly, to complement visual information during compression, we quantize these tokens via a specialized codebook derived from off-the-shelf LLM embeddings to leverage the rich semantics from language modality. Finally, to enhance training stability and convergence, we also introduce a curriculum learning strategy, which proves critical for effective discrete visual representation learning. *SweetTokenizer* achieves comparable video reconstruction fidelity with only **25%** of the tokens used in previous state-of-the-art video tokenizers, and boost video generation results by **32.9%** w.r.t gFVD. When using the same token number, we significantly improves video and image reconstruction results by **57.1%** w.r.t rFVD on UCF-101 and **37.2%** w.r.t rFID on ImageNet-1K. Additionally, the compressed tokens are imbued with semantic information, enabling few-shot recognition capabilities powered by LLMs in downstream applications.

1. Introduction

Visual tokenizers [6, 12, 41, 43, 45, 53, 55] are emerging as essential components in the field of modern computer vision models, particularly in the generation [12, 50, 55] and understanding [18, 28, 36, 44, 47] of vision data. These tools convert visual inputs into discrete tokens, capturing essential temporal and spatial features that facilitate advanced

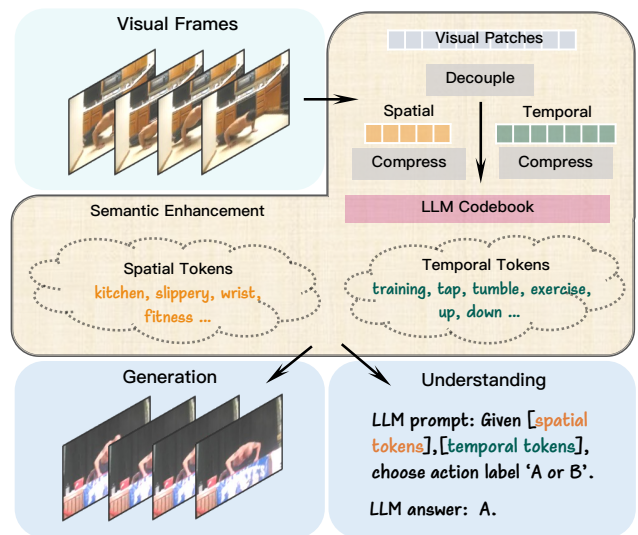


Figure 1. Illustration of our framework. We build a compact visual latent space by reducing token count and leveraging semantic text embedding. The encoded tokens can be applied to downstream tasks, such as generation and understanding.

analysis by formulating visual-related tasks as a token prediction process.

Compression ratio and reconstruction fidelity are vital criteria for evaluating a tokenizer. However, recent visual tokenizers, especially video tokenizers [43, 45, 55] typically retain a low compression ratio. This is because visual tokens are usually derived from 2D patches [10] or 3D tubes [12, 45] which preserve location relationships (e.g., each token corresponds to a specific region of input [56]), leading to redundancy in both spatial and temporal dimensions. To reduce token count, we take inspiration from Q-Former [27], which compresses raw input into learnable “query tokens”. However, it is observed that directly flattening video tokens into sequence may lead to catastrophic temporal information loss. Therefore, we explore a spatial-temporal decoupled approach to perform tokenization.

A higher compression ratio generally makes reconstruction more challenging. To complement visual information during compression, we follow [29, 54, 57] to introduce pretrained language embeddings as the latent codebook, leveraging the powerful semantic representation capabilities of large language models (LLM) [1, 38]. However, previous works primarily focus on image modality, overlooking the relationships between text and motion in video domain.

To address existing limitations, we propose SweetTokenizer – Semantic-aWare spatial-tEmporal Tokenizer – as illustrated in Figure 1. First, considering the heterogeneous redundancy in static images and dynamic frames, we propose the Cross-attention Query AutoEncoder (CQAE) to compress spatial and temporal information into separate learnable queries. Different from previous works [27, 56], our findings indicate that coupling the compression of spatiotemporal information increases the difficulty for the decoder to learn the motion information of the same pixel across consecutive frames. Thus, taking the decoupled spatial and temporal queries as inputs, we devise a strategy of spatial decoding followed by temporal decoding to achieve a separate reconstruction of the spatial and temporal dimensions of visual information. Additionally, the decoupled spatiotemporal reconstruction approach allows for pre-training with a large amount of image data, enhancing the model spatial representation. Second, to integrate the semantic information inherent in large language model (LLM), we design specialized codebooks tailored for spatial and temporal compression addressing the differences in semantic representation between spatial and temporal information. Specifically, we design two language-based codebooks based on the part of speech, using nouns and adjectives for spatial static information and verbs and adverbs for temporal motion information. By incorporating language-based codebooks, the learnable compressed queries can also be easily adapted to downstream visual understanding tasks by in-context learning of LLM. Third, we introduce the curriculum learning [2] mechanism by training SweetTokenizer in three stages to achieve stable convergence. We initially pre-train the spatial CQAE with image data, then joint training of the spatial and temporal CQAE with video data. The first two stages are supervised by the commitment loss of the codebook and the cross-entropy loss of the proxy code [56] from the pretrained tokenizer. In the last stage, we train the whole network and introduce the spatiotemporal decoder to reconstruct the original video.

Exhaustive experiments demonstrate the effectiveness of SweetTokenizer. Compared with SOTA methods [45], SweetTokenizer achieves comparable rFVD on the UCF-101 [34] while utilizing only **25%** of the tokens. Notably, it enhances the gFVD metric from 191 to 128. At an equivalent compression rate on UCF-101, SweetTokenizer reduces rFVD from 42 to 18 and gFVD from 191 to 154. On the

ImageNet-1k [8], SweetTokenizer demonstrates a substantial improvement in rFID, decreasing it from 0.59 to 0.37.

In summary, our work makes the following key contributions:

- We introduce SweetTokenizer, a cutting-edge visual tokenizer that achieves decent reconstruction fidelity with a high compression ratio via spatial-temporal decoupling and cross-attention query autoencoder, reaching a “*sweet spot*” between compression and fidelity.
- We leverage a semantic-enhanced latent codebook to utilize the off-the-shell representation capability of LLM embeddings, which improves reconstruction quality and facilitates downstream video understanding tasks.
- We design a progressive training schedule following the curriculum learning mechanism, which ensures better convergence of visual tokenizers.
- We perform extensive experiments to verify the effectiveness of SweetTokenizer, which exhibits the state-of-the-art performance on video reconstruction, image reconstruction, and class-conditional video generation tasks, leading by a large margin of **57.1%**, **37.2%**, and **32.9%**.

2. Background

2.1. Visual Tokenizer With Vector Quantization

Exploring visual tokenizers and their applications in generative models has led to significant advancements in image/video-related tasks. The general idea is to discretize visual data into tokens, then tasks like visual generation [6, 12, 51, 52] & understanding [4, 10, 18, 19, 28, 36, 44, 47] can be tackled in a sequence prediction style as natural language processing [9, 30, 38]. Our work belongs to the series of Vector Quantized Variational AutoEncoder (VQ-VAE) [32, 41] tokenizers, which introduce a discrete latent space for continuous VAE [22] encoder-decoder structure. It typically encodes a high-dimensional image into a low-dimensional latent representation, then queries the nearest index from a learnable codebook to quantize the latent vector, and finally decodes back reversely to reconstruct the raw input signal. Since this type of tokenizer acquires reconstruction loss, it can maintain high-level semantic and low-level details of input vision. VQGAN [11] adopted adversarial training loss to improve high-frequency details. ViT-VQGAN [51] upgraded encoder-decoder with vision-transformer (ViT) architecture [10] and further boosted results. TiTok [56] replaced 2D image structure with 1D sequence latent representation, then used a self-attention transformer [42] to compress token number.

However, the above methods can only process image data. For video modality, TATS [12] used 3D-CNN to encode video patches and adopted sliding windows to deal with long-term relations. CViViT [43] used ViT [10] structure to encode spatial patches and then adopted a causal

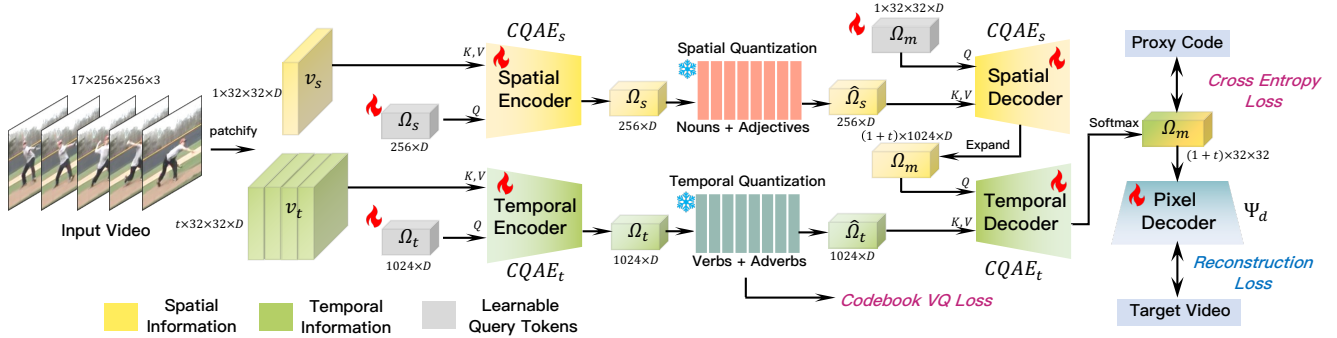


Figure 2. Main pipeline. Our semantic-aware spatial-temporal tokenizer (SweetTokenizer) is trained in a vector-quantized variational autoencoder (VQ-VAE) style. We decouple video into spatial-temporal domains, then encode/decode video via the proposed novel cross-attention query autoencoder (CQAE), which significantly reduces the token number from 5,120 to 1,280 (Section 3.2.2). We further enhance our model with a language-based latent codebook, improving reconstruction fidelity and adding extra semantics (Section 3.2.3). A curriculum learning strategy is adopted to facilitate our training in three stages: Stage 1 and Stage 2 use loss marked purple; Stage 3 uses loss marked blue (Section 3.2.4). The quantized spatial-temporal latent queries $\hat{\Omega}_s, \hat{\Omega}_t$ are used for downstream tasks.

transformer to model temporal information. OmniTokenizer [45] and MAGVIT [53, 55] adopted similar transformer architecture and introduced image pre-training to improve video tokenizer. In this paper, we inherit the popular spatial-temporal decomposition design for video data. Moreover, we significantly increase the token compression ratio with a novel stacked cross-attention query autoencoder, which is inspired by Q-Former [27]’s token compression mechanism.

2.2. Language-based Latent Codebook

The codebooks learned by vanilla VQ-VAEs are not interpretable with lexical meanings. Therefore, many works attempt to utilize pretrained language models embedding codebooks to enhance semantics. LQAE [29] replaced the visual codebook with frozen word embeddings from BERT [9]. SPAE [54] quantized image latent space in a pyramid structure to preserve semantic information from low-level to high-level. It also used large language model (LLM) codebook [7] so that the encoded image token can be directly adapted to visual understanding tasks through in-context learning [3] ability of LLM. We follow this evaluation pipeline for few-shot classification in our paper. V2L-Tokenizer [59] utilized CLIP [31] pretrained encoder and injected a learnable projector to align visual-text latent space implicitly. VQCT [57] replaced the projector with graph convolution networks [24] to consider the relationship between vocabularies. Furthermore, De-Diffusion [48] directly encoded image into plain text as latent space interface and decodes back through a text-to-image (T2I) diffusion model [33]. However, none of these works dives deeply into the codebook design for video modality. Therefore, we propose splitting the codebook according to the video’s spatial-temporal attribute, which uses nouns & adjectives for spatial information, and verbs & adverbs for

temporal information. This design helps us better align visual-motion-text semantics.

3. Method

3.1. Preliminary

A typical visual vector-quantization (VQ) model [12, 45, 53, 55] contains three parts: encoder \mathcal{E} , decoder \mathcal{D} and latent quantizer \mathcal{Q} . Take video modality as an example, given a video input $x \in \mathbb{R}^{T \times H \times W \times 3}$, where T represents the temporal length and $H \times W$ denotes spatial resolution, encoder $\mathcal{E}(x)$ projects it into latent space $\mathbb{Z} \in \mathbb{R}^{N \times D}$, where D is latent dimension and N is token number. A quantizer \mathcal{Q} is constructed in this latent space \mathbb{Z} by querying the nearest neighbor in codebook $C \in \mathbb{R}^{L \times D}$, where L is codebook size. Then \mathcal{D} decodes latent space back to pixel space and applies self-supervised reconstruction loss:

$$\mathcal{L}_{rec}(x, \mathcal{D}(\mathcal{Q}(\mathcal{E}(x))))). \quad (1)$$

We aim to learn a more compact latent space \mathbb{Z} while maintaining the reconstruction fidelity. To this end, we design a semantic-enhanced spatial temporal decoupled tokenizer (SweetTokenizer) to address the issue of token compression (Figure 2). The main component is Cross-attention Query AutoEncoders (CQAE), which aggregates information from disentangled spatial-temporal dimensions into learnable queries, achieving a $4 \times$ compression ratio improvement over previous video modality tokenizers. To enhance latent space representation and reconstruction fidelity, we incorporate compact text embeddings and refine vocabularies by appearance/motion attributes for better semantic alignment. Finally, we propose a progressive training schedule to stabilize convergence.

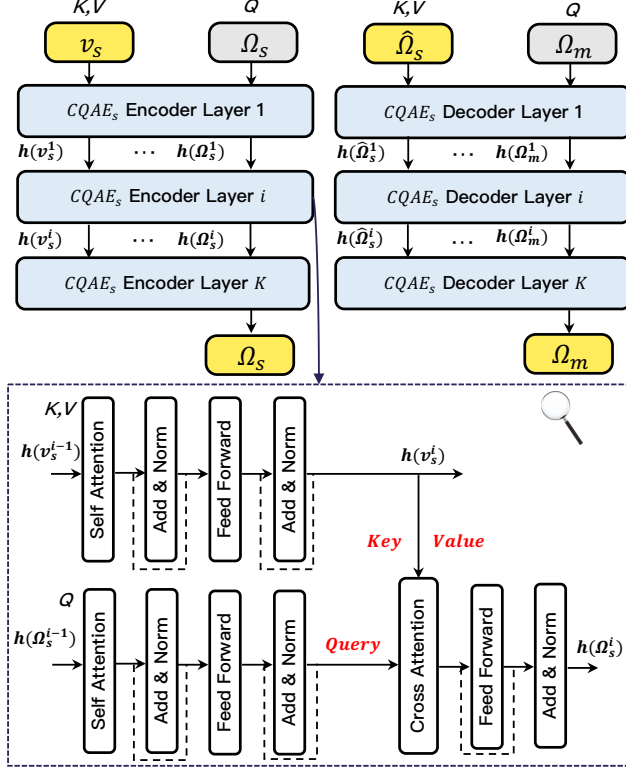


Figure 3. Module structure of Cross-attention Query AutoEncoder (CQAE). Information is transported from K, V head to Q head through stacked CQAE transformer layers. The enlarged view illustrates the detailed architecture.

3.2. Spatial-Temporal Tokenization

3.2.1 Patchify

Given a video frame sequence $x \in \mathbb{R}^{T \times H \times W \times 3}$, we select the first frame x_0 as a reference for spatial information, the remaining $T - 1$ frames $x_{1:T}$ for temporal information, following the strategy in [45]. We apply two patch kernels with shapes $p_h \times p_w$ and $p_t \times p_h \times p_w$ to x_0 and $x_{1:T}$ separately, generating $v_s \in \mathbb{R}^{1 \times \frac{H}{p_h} \times \frac{W}{p_w} \times D}$ and $v_t \in \mathbb{R}^{\frac{T-1}{p_t} \times \frac{H}{p_h} \times \frac{W}{p_w} \times D}$ as inputs for transformer-based autoencoder, where v_s contains spatial information, v_t contains temporal information, with D representing the hidden embedding size. In practice, for a video with 17 frames and a resolution of 256×256 , we set (p_t, p_h, p_w) to $(4, 8, 8)$, thus patchify frames into v_s with shape $1 \times 32 \times 32$ and v_t with shape $4 \times 32 \times 32$. In Figure 2, we use $t = \frac{T-1}{p_t} = 4$ to denote v_t 's length.

3.2.2 Cross-attention Query AutoEncoder (CQAE)

So far, the raw video has been split into patches with a fixed ratio $p_t \times p_h \times p_w$. However, many works [27, 37, 56] have demonstrated that visual information remains redundant spatially and temporally, even after tokenization. To

select “key words” from these tokens, we adopt a strategy similar to Q-Former [27], compressing patch sequence into a fixed number of query tokens via cross-attention interactions. As an innovation, we recursively inject these cross-attention query modules into transformer-based autoencoder to transfer information, forming our CQAE module. Moreover, we show in experiments that naively flattening patches into a long 1D sequence is unsuitable for video modality since it may lose temporal motion information in consecutive frames. Therefore, we introduce two autoencoders, $CQAE_s$ and $CQAE_t$, along with two sets of latent query token embeddings $\Omega_s \in \mathbb{R}^{N_s \times D}$ and $\Omega_t \in \mathbb{R}^{N_t \times D}$, for summarizing spatial and temporal information, where N_s and N_t control the latent token number. We set N_s to 256 and N_t to 1,024, resulting in 1,280 tokens in total.

During the encoding stage, we pass v_s into $CQAE_s$ and v_t into $CQAE_t$. Take $CQAE_s$ as example, as shown in Figure 3, v_s is first reshaped from $1 \times 32 \times 32$ into 1×1024 , then passed through K -layer self-attention transformer to produce K intermediate hidden units $[h(v_s^1), h(v_s^2), \dots, h(v_s^K)]$. Meanwhile, the latent query token Ω_s is also passed through self-attention transformers, except that each hidden unit $h(\Omega_s^i)$ is served as query tensor for cross-attention layer with $h(v_s^i)$. Therefore, we gradually transfer spatial information from v_s into Ω_s through interactions between hidden units $h(v_s^i)$ and $h(\Omega_s)$, reducing the spatial token number from 1,024 to 256.

Similarly, v_t is processed with $CQAE_t$. Instead of directly using v_t , we employ frame-wise residual Δv_t to generate temporal hidden units $[h(\Delta v_t^1), h(\Delta v_t^2), \dots, h(\Delta v_t^K)]$, as [18] found that frame motion residuals can be more effectively represented. Notably, we reshape Δv_t from $4 \times 32 \times 32$ into 1024×4 , and Ω_t from 1024 into 1024×1 to align the transformer inputs shape. Thus, the temporal information is embedded into Ω_t from v_t using the same cross-attention querying approach along the temporal axis. Ω_s and Ω_t are quantized into $\hat{\Omega}_s$ and $\hat{\Omega}_t$, which will be explained in Section 3.2.3 later.

During the decoding stage, we use mask tokens $\Omega_m \in \mathbb{R}^{1 \times \frac{H}{p_h} \times \frac{W}{p_w} \times D}$ to receive information from $\hat{\Omega}_s$ and $\hat{\Omega}_t$, similar to the mask token prediction tasks in [9, 14, 37, 56]. As shown in Figure 3, yellow blocks denote that the tensor contains spatial visual information, while grey blocks indicate that the tensor is information-free. We randomly initialize these mask tokens Ω_m and use them as a “canvas” to reconstruct the raw inputs by receiving visual information from $\hat{\Omega}_s$. The decoding stage consists of two steps. Firstly, the mask token Ω_m starts with shape 32×32 , which is reshaped into 1×1024 to interact spatially with $\hat{\Omega}_s$. Each decoder layer has the same structure as the encoder layer, except that the query is $h(\Omega_m^i)$ and the key/value is $h(\hat{\Omega}_s^i)$. Afterwards, Ω_m is expanded from 1×1024 into 5×1024 , in order to interact temporally with $\hat{\Omega}_t$. The final output Ω_m

is a mixture of yellow and green block as illustrated in Figure 2, indicating that it simultaneously contains spatial and temporal information.

3.2.3 Language-based Latent Codebook

Previous works [29, 54, 57] have shown that text representations can enhance image VQ-VAEs, as the text provides additional semantic information from pre-trained language models. However, previous works mainly focus on the relationship between static image appearance and text semantics. Our experiment in Table 5 shows this is insufficient for video data, as static and motion information are typically embedded in different subsets of vocabularies.

To address this, we construct two separate codebooks, the spatial quantization codebook and the temporal quantization codebook, according to vocabulary attributes, as illustrated in Figure 2. We first extract candidate vocabularies from video captions, which is obtained by Qwen-2.5B [1] instruct model. We filter out words that occur with low frequency. Afterward, we extract Qwen-2.5B [1] text embedding of these vocabularies to fill in the columns of our codebook $C \in \mathbb{R}^{L \times D}$ and split it into four subsets: nouns, adjectives, verbs, and adverbs. Note that C_{noun}, C_{adj} are for spatial latent tokens Ω_s while C_{verb}, C_{adv} are for temporal latent tokens Ω_t .

Given two encoded continuous latent vectors: $z_s \in \Omega_s$ and $z_t \in \Omega_t$, z_s is passed through spatial quantization codebook, and z_t is passed through temporal quantization codebook. The quantized \hat{z}_s and \hat{z}_t are obtained by nearest neighbor searching:

$$z_s, z_t = \mathcal{E}(x), \quad (2)$$

$$\hat{z}_s = \mathcal{P}(c_i), i = \arg \min_{c_i \in C_{noun} \cup C_{adj}} \|z_s - \mathcal{P}(c_i)\|, \quad (3)$$

$$\hat{z}_t = \mathcal{P}(c_i), i = \arg \min_{c_i \in C_{verb} \cup C_{adv}} \|z_t - \mathcal{P}(c_i)\|. \quad (4)$$

To maintain text semantic information, we freeze the codebook and use a tiny projector network \mathcal{P} to map from text space into visual space, following the strategy in [57]. Finally, the gradient is passed to the encoder via vector-quantization commitment loss proposed in [41], a common method to approximate differentiability:

$$\mathcal{L}_{vq} = \|sg[z_s] - \mathcal{Q}(z_s)\|^2 + \|z_s - sg[\mathcal{Q}(z_s)]\|^2 + \|sg[z_t] - \mathcal{Q}(z_t)\|^2 + \|z_t - sg[\mathcal{Q}(z_t)]\|^2 \quad (5)$$

where $sg[\cdot]$ is stop-gradient operator. Figure 4 also shows that the encoded latent words by SweetTokenizer capture semantic meanings related to both visual appearance and motion.

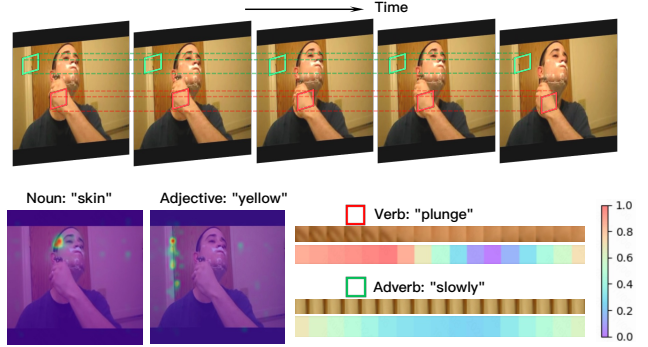


Figure 4. The semantics of spatial-temporal “words”. The attention weights of the last encoder’s cross-attention layer are visualized via heatmap, showing the visual regions corresponding to the related latent words.

3.2.4 Progressive Training Schedule

To ensure better convergence, we follow the philosophy of curriculum learning [2], thus designing a progressive training schedule comprising three stages.

We adopt the proxy codes strategy following [56] to leverage pre-trained visual priors. Assuming $\Psi_e(\cdot)$ is a pre-trained visual tokenizer and $\Psi_d(\cdot)$ is a pre-trained pixel decoder. $\Psi_e(\cdot)$ maps visual inputs x into well-trained integer token indices $\Psi_e(x)$, which serves as a proxy code classification label of our CQAE model, similar to the knowledge distilling approach [16]. The motivation is that we could bypass the early oscillatory training phase of GAN loss [13] as demonstrated in [11, 56], which allows us to apply it later once the training becomes stable. In practice, we use OmniTokenizer [45]’s encoder and decoder as $\Psi_e(\cdot)$ and $\Psi_d(\cdot)$.

First, we train $CQAE_s$ on spatial patches v_s using image data only as pre-training in **Stage 1**, with the supervision of proxy code:

$$\mathcal{L}_{stage1} = \mathcal{L}_c(CQAE_s(v_s), \Psi_e(x)) + \mathcal{L}_{vq}, \quad (6)$$

where \mathcal{L}_c denotes cross entropy loss and \mathcal{L}_{vq} denotes codebook commitment loss in Eq 5. Note that SweetTokenizer adopts spatial-temporal disentanglement, so the model weights of $CQAE_s$ can be later adapted to image-level tasks via finetuning. Experiments in Table 3 show that our spatial branch already achieves satisfactory image reconstruction results.

Second, we jointly train $CQAE_s, CQAE_t$ on v_s, v_t using video data in **Stage 2**. Since $CQAE_s$ is well-initialized, $CQAE_t$ can focus on learning temporal motions:

$$\mathcal{L}_{stage2} = \mathcal{L}_c(CQAE_s(v_s), \Psi_e(x)) + \mathcal{L}_c(CQAE_t(v_t), \Psi_e(x)) + \mathcal{L}_{vq}. \quad (7)$$

Finally, in **Stage 3**, we combine the pre-trained pixel decoder $\Psi_d(\cdot)$ together with our CQAE and finetune them by

| Tokenizer | #Tokens | rFVD ↓ | |
|--------------------|------------|-----------|----------|
| | | UCF-101 | K-600 |
| MaskGIT [6] | 4352 | 240 | 202 |
| VQGAN [11] | 4352 | 299 | 270 |
| TATS [12] | 4096 | 162 | - |
| MAGVIT [53] | 4096 | 58 | - |
| OmniTokenizer [45] | 5120 | 42 | 26 |
| SweetTokenizer* | 5120 | 18 | 8 |
| SweetTokenizer | 256 + 1024 | 44 | 28 |

Table 1. Video reconstruction FVD on the UCF-101 and K-600 dataset, using a frame resolution 256×256 . “*” denotes training SweetTokenizer without token compression.

| Tokenizer | #Params | #Tokens | gFVD ↓ |
|--------------------|---------|------------|------------|
| CogVideo [17] | 9.4B | 6800 | 626 |
| TATS [12] | 321M | 4096 | 332 |
| Video-LaVIT [18] | 7B | 512 | 280 |
| OmniTokenizer [45] | 650M | 5120 | 191 |
| SweetTokenizer* | 650M | 5120 | 154 |
| SweetTokenizer | 650M | 256 + 1024 | 128 |

Table 2. Comparison of class-conditional generation results on UCF-101. Each video is composed of 17 frames with a resolution of 256×256 . We only compare autoregressive generators (AR) as baselines. “#Params” refers the parameter number of generator.

pixel-level losses in Stage 3 to boost final performance:

$$\mathcal{L}_{stage3} = \mathcal{L}_{(m,g,p)}(\Psi_d(CQAE(v)), x), \quad (8)$$

where \mathcal{L}_m denotes mean-squared error loss, \mathcal{L}_g denotes GAN loss [13] and \mathcal{L}_p denotes perceptual loss [20].

4. Experiments

4.1. Experiments Settings

Dataset. We evaluate the tokenization performance of SweetTokenizer on image and video datasets, including ImageNet [8], UCF-101 [34], and Kinetics-600 [5, 21]. Following [45], all images and video frames are resized to 256×256 resolution for experiments. The semantic capabilities of SweetTokenizer are tested through few-shot image classification on Real-Name Open-Ended miniImageNet [39] and few-shot video action recognition on UCF-101, as described in [58].

Evaluation Metrics. For video reconstruction experiments, we evaluate using the Reconstruction Frchet Video Distance (rFVD) [40]. For video generation, we use the Generation Frchet Video Distance (gFVD) metric. For image reconstruction, we categorize recent methods by the number of compressed tokens, with each group assessed using the Frchet Inception Distance (FID) [15].

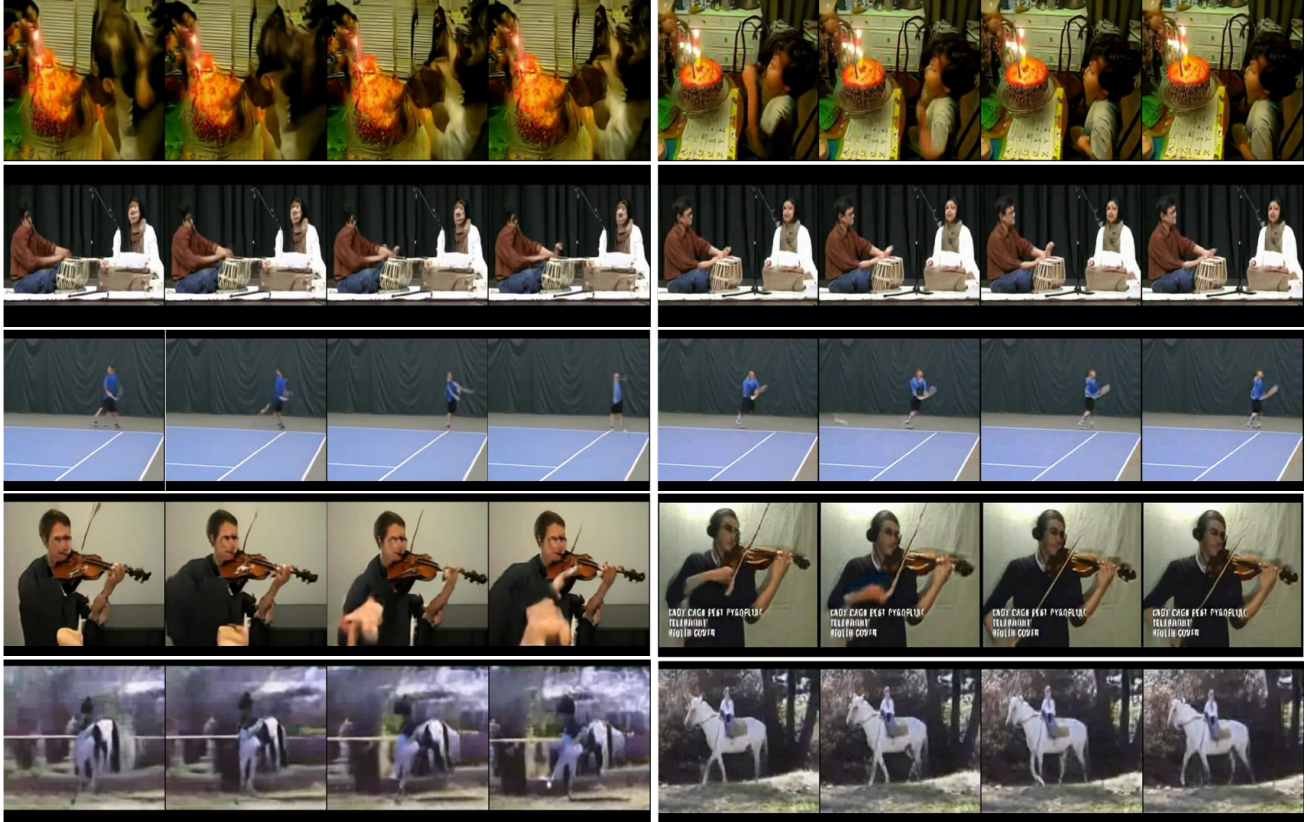
| Tokenizer | #Tokens | Codebook Size | rFID ↓ |
|---------------------------------|---------|---------------|-------------|
| VQGAN [11] | 256 | 1024 | 7.94 |
| RQ-VAE [26] | 256 | 16384 | 3.20 |
| MaskGIT[53] | 256 | 1024 | 2.28 |
| LlamaGen-16 [35] | 256 | 16384 | 2.19 |
| TiTok [56] | 256 | 4096 | 1.03 |
| SweetTokenizer | 256 | 10481 | 0.73 |
| ViT-VQGAN [51] | 1024 | 8192 | 1.28 |
| OmniTokenizer [45] | 1024 | 8192 | 1.11 |
| OmniTokenizer [◊] [45] | 1024 | 8192 | 0.69 |
| LlamaGen-8 [35] | 1024 | 16384 | 0.59 |
| SweetTokenizer* | 1024 | 10481 | 0.37 |

Table 3. Image reconstruction FID on the ImageNet dataset, using a resolution of 256×256 . “◊” denotes continuous latent space without quantization. “*” denotes training SweetTokenizer without token compression.

Implementation Details. SweetTokenizer adopts a spatial-temporal architecture consisting of 8 spatial layers and 4 temporal layers, with both the encoder and decoder configured to a hidden dimension of 512. The latent space dimension is set to 256. For the LLM codebook quantizer, we exclude words with a frequency below 5, resulting in a selection of 5,078 nouns, 5,403 adjectives, 9,267 verbs, and 1,872 adverbs. This forms a spatial codebook of size 10,481 and a temporal codebook of size 11,139. We utilize a graph convolution network (GCN) to project Qwen-2.5 embeddings [1] into the visual latent space. Graph edges are constructed when a pair of words co-occur within a 5-token window in the text. The model is trained with a progressive three-stage schedule: Stage 1 uses a batch size of 32 for 300K iterations, Stage 2 uses a batch size of 8 for 300K iterations, and Stage 3 uses a batch size of 4 for 500K iterations. All training is performed on NVIDIA A100 GPUs. Adam [23] is employed for optimization ($\beta_1 = 0.9$ and $\beta_2 = 0.99$). During each stage, we use a cosine learning rate scheduler with a max learning rate of $1e-4$ and a min learning rate of $1e-5$, warmed up by 10K iterations.

4.2. Video Reconstruction & Generation

We first evaluate the tokenization capability of SweetTokenizer on the UCF-101 and K-600 video datasets. As shown in Table 1, SweetTokenizer uses only 1,280 tokens (256 spatial tokens and 1,024 temporal tokens), which is four times fewer than OmniTokenizer’s 5,120 tokens. Despite this significant reduction, it achieves comparable performance, with rFVD scores of 44.35 on UCF-101 and 27.95 on K-600, demonstrating its effectiveness in compressing tokens while maintaining high fidelity. Notably, at the same compression ratio, SweetTokenizer* significantly outperforms all baselines, achieving an rFVD of 18.74 on UCF-101,



OmniTokenizer [45]

SweetTokenizer (ours)

Figure 5. Class-conditional video generation result using OmniTokenizer [45] and our SweetTokenizer, on UCF-101 dataset. The action class label of each row is: “BlowingCandles”, “PlayingTabla”, “TennisSwing”, “PlayingViolin” and “HorseRiding”.

57.1% lower than OmniTokenizer’s 42.35, and an rFVD of 7.51 on K-600, 71.0% lower than OmniTokenizer’s 25.97.

The generative capability of SweetTokenizer is evaluated on UCF-101 in a class-conditional generation task. SweetTokenizer is used to extract quantized spatial tokens ($\hat{\Omega}_s$) and temporal tokens ($\hat{\Omega}_t$) from UCF videos. These tokens are then concatenated to form training sequences for a 24-layer autoregressive (AR) transformer [49], following the same generation protocol as OmniTokenizer. As shown in Table 2, SweetTokenizer achieves a significant performance improvement, with a gFVD score of 128, 32.9% lower than OmniTokenizer’s 191 gFVD. This improvement is attributed to SweetTokenizer’s effective token compression, which substantially reduces the training complexity for downstream autoregressive models.

The visualization results are presented in Figure 5. To ensure a fair comparison, we select generated videos with similar appearances, as the generation process inherently involves randomness. The results demonstrate significantly improved detail, such as clearer human facial features and finer table textures. Additionally, SweetTokenizer effectively preserves temporal consistency, even under large motion scenarios. Further quantitative and qualitative results

on video datasets are provided in the supplementary.

4.3. Image Reconstruction

We evaluate the image tokenization performance of SweetTokenizer on ImageNet by fine-tuning the spatial branch $CQAE_s$ with a pixel-level loss during Stage 3. As shown in Table 3, we compare SweetTokenizer with recent methods under various token compression settings. With 256 spatial tokens, SweetTokenizer outperforms TiTok [56] by 27.8%, reducing rFID from 1.01 to 0.73. When using 1,024 spatial tokens, SweetTokenizer* achieves a significant improvement over both VQ-based and non-VQ-based methods (marked \diamond), achieving an rFID of 0.37, which surpasses LlamaGen-8 [35] by 37.3%. More quantitative and qualitative results on image reconstruction and generation tasks are shown in the supplementary.

4.4. Ablation Studies

Spatial-Temporal Decoupling. We demonstrate that naively flattening video tokens into a 1D sequence is infeasible, as shown in Table 4. Training SweetTokenizer without decoupling results in significantly degraded performance. We attribute this degradation to two factors: (1) the

| Architecture & Training Schedule | rFVD ↓ |
|---|--------------|
| Stage2 w/o decoupling | 892.70 |
| Stage2 | 501.12 |
| Stage2 + Stage3 | 269.34 |
| Stage1 + Stage2 | 155.92 |
| Stage1 + Stage2 + Stage3 (SweetTokenizer) | 44.35 |

Table 4. Ablation study of spatial-temporal decoupling and progressive training schedule.

| UCF-101 | rFVD ↓ |
|---|--------------|
| Baseline (w/o LLC) | 67.94 |
| + Spatial LLC | 55.11 |
| + Spatial & Temporal LLC (SweetTokenizer) | 44.35 |
| + CLIP [31]-based LLC | 45.56 |
| + Qwen [1]-based LLC (SweetTokenizer) | 44.35 |
| ImageNet | rFID ↓ |
| Baseline (w/o LLC) | 1.26 |
| + Spatial LLC (SweetTokenizer) | 0.73 |

Table 5. Ablation study of language-based latent codebook (LLC) settings on UCF-101 and ImageNet.

flattening operation discards substantial consecutive temporal information, and (2) without decoupling, the model cannot leverage the crucial spatial pretraining from large-scale image datasets, as further discussed in the next paragraph.

Progressive Training Schedule. This paragraph highlights the advantages of our progressive training schedule for the model, evaluated on the UCF-101 dataset. The results, presented in Table 4, demonstrate the critical role of each training stage. First, we underscore the importance of spatial training: omitting Stage 1 results in significantly poor rFVD scores of 269.34 and 501.12 for the combinations of “Stage 2 + Stage 3” and “Stage 2” alone, respectively. Secondly, the proxy code finetuning strategy employed in Stage 3 has a substantial impact on overall performance, improving the rFVD score from 155.92 with “Stage 1 + Stage 2” to 44.35 with the full sequence of “Stage 1 + Stage 2 + Stage 3”. These findings highlight the necessity of our complete progressive learning schedule, as each stage contributes to enhancing the model performance.

Language-based Latent Codebook. We evaluate the impact of our architecture design on model performance, focusing on the effects of the spatial-temporal language-based latent codebooks (LLC) on the ImageNet and UCF-101 datasets. As illustrated in Table 5, the integration of the spatial language codebook consistently enhances performance across both video and image modalities, improving the rFVD score from 67.94 to 55.11 and the rFID score from 1.26 to 0.73. Moreover, our temporal language codebook significantly benefits video reconstruction tasks, fur-

| Methods | ImageNet | | | | UCF-101 | |
|----------------|--------------|-------------|-------------|-------------|---------|-------------|
| | K-way-N-shot | 2-1 | 2-3 | 2-5 | Avg | 5-5 |
| SPAE [54] | 84.8 | 92.5 | 92.6 | 89.9 | - | - |
| V2L [59] | 76.3 | 91.2 | 95.3 | 87.6 | - | - |
| ARN[58] | - | - | - | - | - | 83.1 |
| HF-AR [25] | - | - | - | - | - | 86.4 |
| SweetTokenizer | 86.8 | 90.5 | 95.2 | 90.8 | - | 90.1 |

Table 6. Few-shot visual classification accuracy (↑), evaluated on both image and video modality.

ther reducing the rFVD score from 55.11 to 44.35. This underscores the importance of our unique design for video modalities. We attribute these improvements to the robust semantic features provided by language-based embeddings and their inherent alignment between visual and text spaces. Additionally, we compare different types of language-based embeddings, such as using CLIP [31] embeddings in place of Qwen-2.5B [1] embeddings. The experiments indicate that while CLIP embeddings yield satisfactory results, employing a more powerful pre-trained language model leads to superior performance.

4.5. Visual Semantic Comprehension

Few-Shot Visual Classification. To evaluate the semantic capabilities of SweetTokenizer, we conducted experiments on few-shot image classification and video action recognition tasks. In both experiments, we initially extracted visual tokens using SweetTokenizer and transformed them into natural language words via our LLM codebook. Subsequently, we employed CLIP to compute the similarity between the visual inputs and text embeddings. The top 21 tokens with the highest similarity were selected to form a prompt for prediction using the Qwen LLM. For the image classification task, we adhered to the V2L protocol [59], comparing SweetTokenizer against other language-based visual tokenizers SPAE [54] and V2L. In the video action recognition task, we used ARN [58] and HF-AR [25] as baselines. The results in Table 6 indicate that SweetTokenizer achieved an accuracy of 90.8% on the miniImageNet dataset, surpassing SPAE 89.9% and V2L 87.6%. On the UCF-101 dataset, SweetTokenizer attain an average accuracy of 90.1%, outperforming ARN 83.1% and HF-AR 86.4%. These findings demonstrate SweetTokenizer robust semantic understanding and superior performance in both image and video tasks.

5. Conclusions

We present SweetTokenizer, an efficient visual tokenization framework that compresses spatial and temporal information through the cross-attention query autoencoder. Combined with language-based latent spaces and progressive training schedule, SweetTokenizer reduces token count by

4× for video data while maintaining high reconstruction fidelity. Our approach offers a compact representation of visual data, making it well-suited for downstream tasks such as visual generation, visual recognition, marking a significant step in efficient visual tokenization.

References

- [1] Jinze Bai, Shuai Bai, Yunfei Chu, Zeyu Cui, Kai Dang, Xiaodong Deng, Yang Fan, Wenbin Ge, Yu Han, Fei Huang, et al. Qwen technical report. [arXiv preprint arXiv:2309.16609](#), 2023. [2](#), [5](#), [6](#), [8](#)
- [2] Yoshua Bengio, Jérôme Louradour, Ronan Collobert, and Jason Weston. Curriculum learning. In [ICML](#), 2009. [2](#), [5](#)
- [3] Tom B Brown. Language models are few-shot learners. [arXiv preprint arXiv:2005.14165](#), 2020. [3](#)
- [4] Nicolas Carion, Francisco Massa, Gabriel Synnaeve, Nicolas Usunier, Alexander Kirillov, and Sergey Zagoruyko. End-to-end object detection with transformers. In [European conference on computer vision](#), pages 213–229. Springer, 2020. [2](#)
- [5] Joao Carreira, Eric Noland, Andras Banki-Horvath, Chloe Hillier, and Andrew Zisserman. A short note about kinetics-600. [arXiv preprint arXiv:1808.01340](#), 2018. [6](#)
- [6] Huiwen Chang, Han Zhang, Lu Jiang, Ce Liu, and William T Freeman. Maskgit: Masked generative image transformer. In [CVPR](#), pages 11315–11325, 2022. [1](#), [2](#), [6](#)
- [7] Aakanksha Chowdhery, Sharan Narang, Jacob Devlin, Maarten Bosma, Gaurav Mishra, Adam Roberts, Paul Barham, Hyung Won Chung, Charles Sutton, Sebastian Gehrmann, et al. Palm: Scaling language modeling with pathways. [JMLR](#), 24(240):1–113, 2023. [3](#)
- [8] Jia Deng, Wei Dong, Richard Socher, Li-Jia Li, Kai Li, and Li Fei-Fei. Imagenet: A large-scale hierarchical image database. In [2009 IEEE conference on computer vision and pattern recognition](#), pages 248–255. Ieee, 2009. [2](#), [6](#)
- [9] Jacob Devlin. Bert: Pre-training of deep bidirectional transformers for language understanding. [NAACL](#), 2018. [2](#), [3](#), [4](#)
- [10] Alexey Dosovitskiy. An image is worth 16x16 words: Transformers for image recognition at scale. [ICLR](#), 2020. [1](#), [2](#)
- [11] Patrick Esser, Robin Rombach, and Björn Ommer. Taming transformers for high-resolution image synthesis, 2021. [2](#), [5](#), [6](#), [1](#)
- [12] Songwei Ge, Thomas Hayes, Harry Yang, Xi Yin, Guan Pang, David Jacobs, Jia-Bin Huang, and Devi Parikh. Long video generation with time-agnostic vqgan and time-sensitive transformer. In [European Conference on Computer Vision](#), pages 102–118. Springer, 2022. [1](#), [2](#), [3](#), [6](#)
- [13] Ian J. Goodfellow, Jean Pouget-Abadie, Mehdi Mirza, Bing Xu, David Warde-Farley, Sherjil Ozair, Aaron Courville, and Yoshua Bengio. Generative adversarial networks, 2014. [5](#), [6](#)
- [14] Kaiming He, Xinlei Chen, Saining Xie, Yanghao Li, Piotr Dollár, and Ross Girshick. Masked autoencoders are scalable vision learners. In [CVPR](#), pages 16000–16009, 2022. [4](#)
- [15] Martin Heusel, Hubert Ramsauer, Thomas Unterthiner, Bernhard Nessler, and Sepp Hochreiter. Gans trained by a two time-scale update rule converge to a local nash equilibrium. [Advances in neural information processing systems](#), 30, 2017. [6](#)
- [16] Geoffrey Hinton. Distilling the knowledge in a neural network. [NeurIPS Workshop](#), 2014. [5](#)
- [17] Wenyi Hong, Ming Ding, Wendi Zheng, Xinghan Liu, and Jie Tang. Cogvideo: Large-scale pretraining for text-to-video generation via transformers. [arXiv preprint arXiv:2205.15868](#), 2022. [6](#)
- [18] Yang Jin, Zhicheng Sun, Kun Xu, Liwei Chen, Hao Jiang, Quzhe Huang, Chengru Song, Yuliang Liu, Di Zhang, Yang Song, Kun Gai, and Yadong Mu. Video-lavit: Unified video-language pre-training with decoupled visual-motional tokenization. In [ICML](#), pages 22185–22209, 2024. [1](#), [2](#), [4](#), [6](#)
- [19] Yang Jin, Kun Xu, Kun Xu, Liwei Chen, Chao Liao, Jianchao Tan, Yadong Mu, et al. Unified language-vision pre-training in llm with dynamic discrete visual tokenization. In [ICLR](#), 2024. [2](#)
- [20] Justin Johnson, Alexandre Alahi, and Li Fei-Fei. Perceptual losses for real-time style transfer and super-resolution. In [ECCV](#), pages 694–711. Springer, 2016. [6](#)
- [21] Will Kay, Joao Carreira, Karen Simonyan, Brian Zhang, Chloe Hillier, Sudheendra Vijayanarasimhan, Fabio Viola, Tim Green, Trevor Back, Paul Natsev, et al. The kinetics human action video dataset. [arXiv preprint arXiv:1705.06950](#), 2017. [6](#)
- [22] Diederik P Kingma. Auto-encoding variational bayes. [ICLR](#), 2013. [2](#)
- [23] Diederik P Kingma. Adam: A method for stochastic optimization. [arXiv preprint arXiv:1412.6980](#), 2014. [6](#)
- [24] Thomas N Kipf and Max Welling. Semi-supervised classification with graph convolutional networks. [ICLR](#), 2016. [3](#)
- [25] Neeraj Kumar and Siddhansh Narang. Few shot activity recognition using variational inference. [arXiv preprint arXiv:2108.08990](#), 2021. [8](#)
- [26] Doyup Lee, Chiheon Kim, Saehoon Kim, Minsu Cho, and Wook-Shin Han. Autoregressive image generation using residual quantization. In [Proceedings of the IEEE/CVF Conference on Computer Vision and Pattern Recognition](#), pages 11523–11532, 2022. [6](#), [1](#)
- [27] Junnan Li, Dongxu Li, Silvio Savarese, and Steven Hoi. Blip-2: Bootstrapping language-image pre-training with frozen image encoders and large language models. In [ICML](#), pages 19730–19742, 2023. [1](#), [2](#), [3](#), [4](#)
- [28] Bin Lin, Bin Zhu, Yang Ye, Munan Ning, Peng Jin, and Li Yuan. Video-llava: Learning united visual representation by alignment before projection. 2023. [1](#), [2](#)
- [29] Hao Liu, Wilson Yan, and Pieter Abbeel. Language quantized autoencoders: Towards unsupervised text-image alignment. [NeurIPS](#), 36, 2023. [2](#), [3](#), [5](#)
- [30] Alec Radford, Jeffrey Wu, Rewon Child, David Luan, Dario Amodei, Ilya Sutskever, et al. Language models are unsupervised multitask learners. [OpenAI blog](#), 1(8):9, 2019. [2](#)
- [31] Alec Radford, Jong Wook Kim, Chris Hallacy, Aditya Ramesh, Gabriel Goh, Sandhini Agarwal, Girish Sastry,

- Amanda Askeell, Pamela Mishkin, Jack Clark, et al. Learning transferable visual models from natural language supervision. In *ICML*, pages 8748–8763, 2021. 3, 8
- [32] Ali Razavi, Aaron Van den Oord, and Oriol Vinyals. Generating diverse high-fidelity images with vq-vae-2. *NeurIPS*, 32, 2019. 2, 1
- [33] Robin Rombach, Andreas Blattmann, Dominik Lorenz, Patrick Esser, and Björn Ommer. High-resolution image synthesis with latent diffusion models, 2021. 3
- [34] K Soomro. Ucf101: A dataset of 101 human actions classes from videos in the wild. *arXiv preprint arXiv:1212.0402*, 2012. 2, 6
- [35] Peize Sun, Yi Jiang, Shoufa Chen, Shilong Zhang, Bingyue Peng, Ping Luo, and Zehuan Yuan. Autoregressive model beats diffusion: Llama for scalable image generation. *arXiv preprint arXiv:2406.06525*, 2024. 6, 7
- [36] Quan Sun, Qiying Yu, Yufeng Cui, Fan Zhang, Xiaosong Zhang, Yueze Wang, Hongcheng Gao, Jingjing Liu, Tiejun Huang, and Xinlong Wang. Generative pretraining in multimodality. *ICLR*, 2024. 1, 2
- [37] Zhan Tong, Yibing Song, Jue Wang, and Limin Wang. Videomae: Masked autoencoders are data-efficient learners for self-supervised video pre-training. *NeurIPS*, 35:10078–10093, 2022. 4
- [38] Hugo Touvron, Thibaut Lavril, Gautier Izacard, Xavier Martinet, Marie-Anne Lachaux, Timothée Lacroix, Baptiste Rozière, Naman Goyal, Eric Hambro, Faisal Azhar, et al. Llama: Open and efficient foundation language models. *arXiv preprint arXiv:2302.13971*, 2023. 2
- [39] Maria Tsimpoukelli, Jacob L Menick, Serkan Cabi, SM Eslami, Oriol Vinyals, and Felix Hill. Multimodal few-shot learning with frozen language models. *Advances in Neural Information Processing Systems*, 34:200–212, 2021. 6
- [40] Thomas Unterthiner, Sjoerd Van Steenkiste, Karol Kurach, Raphael Marinier, Marcin Michalski, and Sylvain Gelly. Towards accurate generative models of video: A new metric & challenges. *arXiv preprint arXiv:1812.01717*, 2018. 6
- [41] Aaron Van Den Oord, Oriol Vinyals, et al. Neural discrete representation learning. *Advances in neural information processing systems*, 30, 2017. 1, 2, 5
- [42] A Vaswani. Attention is all you need. *NeurIPS*, 2017. 2
- [43] Ruben Villegas, Mohammad Babaeizadeh, Pieter-Jan Kindermans, Hernan Moraldo, Han Zhang, Mohammad Taghi Saffar, Santiago Castro, Julius Kunze, and Dumitru Erhan. Phenaki: Variable length video generation from open domain textual descriptions. In *ICLR*, 2023. 1, 2
- [44] Junke Wang, Dongdong Chen, Chong Luo, Bo He, Lu Yuan, Zuxuan Wu, and Yu-Gang Jiang. Omnivid: A generative framework for universal video understanding. In *CVPR*, pages 18209–18220, 2024. 1, 2
- [45] Junke Wang, Yi Jiang, Zehuan Yuan, Binyue Peng, Zuxuan Wu, and Yu-Gang Jiang. Omnitokenizer: A joint image-video tokenizer for visual generation. *NeurIPS*, 2024. 1, 2, 3, 4, 5, 6, 7
- [46] Rui Wang, Dongdong Chen, Zuxuan Wu, Yinpeng Chen, Xiyang Dai, Mengchen Liu, Yu-Gang Jiang, Luowei Zhou, and Lu Yuan. Bevt: Bert pretraining of video transformers. In *Proceedings of the IEEE/CVF conference on computer vision and pattern recognition*, pages 14733–14743, 2022. 1
- [47] Yi Wang, Kunchang Li, Xinhao Li, Jiashuo Yu, Yanan He, Guo Chen, Baoqi Pei, Rongkun Zheng, Jilan Xu, Zun Wang, et al. Internvideo2: Scaling video foundation models for multimodal video understanding. *ECCV*, 2024. 1, 2
- [48] Chen Wei, Chenxi Liu, Siyuan Qiao, Zhishuai Zhang, Alan Yuille, and Jiahui Yu. De-diffusion makes text a strong cross-modal interface. In *CVPR*, pages 13492–13503, 2024. 3
- [49] Wilson Yan, Yunzhi Zhang, Pieter Abbeel, and Aravind Srinivas. Videogpt: Video generation using vq-vae and transformers. *arXiv preprint arXiv:2104.10157*, 2021. 7
- [50] Jaehoon Yoo, Semin Kim, Doyup Lee, Chiheon Kim, and Seunghoon Hong. Towards end-to-end generative modeling of long videos with memory-efficient bidirectional transformers. In *CVPR*, pages 22888–22897, 2023. 1
- [51] Jiahui Yu, Xin Li, Jing Yu Koh, Han Zhang, Ruoming Pang, James Qin, Alexander Ku, Yuanzhong Xu, Jason Baldridge, and Yonghui Wu. Vector-quantized image modeling with improved vqgan. *ICLR*, 2022. 2, 6
- [52] Jiahui Yu, Yuanzhong Xu, Jing Yu Koh, Thang Luong, Gungjan Baid, Zirui Wang, Vijay Vasudevan, Alexander Ku, Yinfei Yang, Burcu Karagol Ayan, et al. Scaling autoregressive models for content-rich text-to-image generation. *ICLR*, 2024. 2
- [53] Lijun Yu, Yong Cheng, Kihyuk Sohn, José Lezama, Han Zhang, Huiwen Chang, Alexander G Hauptmann, Ming-Hsuan Yang, Yuan Hao, Irfan Essa, and Lu Jiang. MAGVIT: Masked generative video transformer. In *CVPR*, 2023. 1, 3, 6
- [54] Lijun Yu, Yong Cheng, Zhiruo Wang, Vivek Kumar, Wolfgang Macherey, Yanping Huang, David Ross, Irfan Essa, Yonatan Bisk, Ming-Hsuan Yang, et al. Spae: Semantic pyramid autoencoder for multimodal generation with frozen llms. *NeurIPS*, 36, 2023. 2, 3, 5, 8
- [55] Lijun Yu, José Lezama, Nitesh B Gundavarapu, Luca Versari, Kihyuk Sohn, David Minnen, Yong Cheng, Vighnesh Birodkar, Agrim Gupta, Xiuye Gu, et al. Language model beats diffusion–tokenizer is key to visual generation. *ICLR*, 2023. 1, 3
- [56] Qihang Yu, Mark Weber, Xueqing Deng, Xiaohui Shen, Daniel Cremers, and Liang-Chieh Chen. An image is worth 32 tokens for reconstruction and generation. *NeurIPS*, 2024. 1, 2, 4, 5, 6, 7
- [57] Baoquan Zhang, Huaibin Wang, Chuyao Luo, Xutao Li, Guotao Liang, Yunming Ye, Xiaochen Qi, and Yao He. Codebook transfer with part-of-speech for vector-quantized image modeling. In *CVPR*, pages 7757–7766, 2024. 2, 3, 5
- [58] Hongguang Zhang, Li Zhang, Xiaojuan Qi, Hongdong Li, Philip HS Torr, and Piotr Koniusz. Few-shot action recognition with permutation-invariant attention. In *ECCV*, pages 525–542. Springer, 2020. 6, 8
- [59] Lei Zhu, Fangyun Wei, and Yanye Lu. Beyond text: Frozen large language models in visual signal comprehension. In *CVPR*, pages 27047–27057, 2024. 3, 8

SweetTokenizer: Semantic-Aware Spatial-Temporal Tokenizer for Compact Visual Discretization

Supplementary Material

| Notations | Explanations |
|----------------------------|------------------------------------|
| $CQAE_{s,t}$ | Cross-attention query autoencoder |
| \mathcal{E} | Encoder |
| \mathcal{D} | Decoder |
| \mathcal{Q} | Quantizer |
| $p_{t,h,w}$ | Downsample ratio |
| $\Omega_{s,t,m}$ | Continuous latent query tokens |
| $z_{s,t,m}$ | Continuous latent query token |
| $\hat{\Omega}_{s,t}$ | Quantized latent query tokens |
| $\hat{z}_{s,t}$ | Quantized latent query token |
| $v_{s,t}$ | Continuous visual feature |
| $\hat{v}_{s,t}$ | Discrete visual feature |
| $h(\cdot)$ | Hidden unit |
| Δv | Difference of consecutive features |
| $C_{adj,noun,adverb,verb}$ | Codebook text embeddings |
| $c_{adj,noun,adverb,verb}$ | Codebook text embedding |
| \mathcal{P} | Projector network |
| $sg(\cdot)$ | Stop gradient operation |
| $\Psi_{e,d}(\cdot)$ | Pretrained encoder & decoder |
| \mathcal{L}_c | Cross-Entropy loss |
| \mathcal{L}_{vq} | Commitment loss |
| \mathcal{L}_m | Mean-squared loss |
| \mathcal{L}_g | Gan loss |
| \mathcal{L}_p | Perceptual loss |

Table 7. Explanations for the notations in the main paper.

6. Experimental Settings

6.1. Model Implementation Details

Visual Tokenizer. The tokenizer is composed of an encoder \mathcal{E} , decoder \mathcal{D} , and latent quantizer \mathcal{Q} . The tokenizer takes a video clip of 17 consecutive frames with a resolution of 256×256 with the elements normalized to $[-0.5, 0.5]$ as input. Then the video clip will be patchified to a resolution of $1 \times 32 \times 32$ spatial feature and $4 \times 32 \times 32$ temporal feature as illustrated in the main paper. The encoder \mathcal{E} and decoder \mathcal{D} in our tokenizer are both composed of 8 $CQAE_s$ modules and 4 $CQAE_t$ modules with 512 hidden states and 8 attention heads. Each modules consists of self-attention, feed-forward and cross-attention layers. Before the attention computation, the visual features will be reshaped into $[(BT) \times (HW) \times D]$ and $[(BHW) \times T \times D]$ for $CQAE_s$ and $CQAE_t$ modules, respectively. The encoder \mathcal{E} generates 256 spatial and 1024 temporal continuous latent tokens. These tokens are then passed to the quantizer \mathcal{Q} , which produces the quantized spatial and temporal latent tokens. The

| Tokenizer | #Params | #Tokens | FID ↓ |
|---------------------|---------|---------|-------------|
| VQVAE-2 [32] | 13.5B | 1024 | 31.11 |
| VQGAN [11] | 1.4B | 1024 | 74.3 |
| RQ-Transformer [26] | 821M | 1024 | 13.11 |
| ViT-VQGAN [46] | 650M | 1024 | 8.81 |
| OmniTokenizer [45] | 650M | 1024 | 7.45 |
| SweetTokenizer | 650M | 256 | 5.48 |

Table 8. Comparison of class-conditional generation results on ImageNet-1K. Each image is of resolution of 256×256 . We only compare autoregressive generators (AR) as baselines. “#Params” refers the parameter number of generator.

quantizer \mathcal{Q} is composed of a spatial and temporal codebook and a GCN with two hidden layers with hidden dimension of 512 as the projector network \mathcal{P} . To improve the training stability of the visual tokenizer, we adopt exponential moving average (EMA) updates with weight of 0.999 following [56].

Language Model. We utilize VideoGPT following [45] as the default large language model for the video generative pre-training. All settings follow the protocol of [45].

6.2. Training Datasets

UCF-101. UCF-101 is a large-scale action recognition dataset consisting of 13,320 videos with 9537 for training and 3783 for testing across 101 action categories. The dataset includes videos with significant variations in camera motion, object appearance, scale, viewpoint, cluttered backgrounds, and lighting conditions, making it one of the most challenging datasets for action recognition.

Kinetic-600. Kinetics-600 is a large-scale action recognition dataset containing approximately 480K videos across 600 action categories. The dataset is split into 390K training, 30K validation, and 60K test videos. Each video is a 10-second clip extracted from raw YouTube footage, focusing on key action moments.

ImageNet-1K. ImageNet-1K is a widely used subset of the larger ImageNet dataset, specifically designed for image classification tasks. It contains 1.2 million labeled images across 1,000 distinct categories, ranging from animals and plants to everyday objects and scenes. Each category in ImageNet-1K includes a set of training images, along with

| Configuration | Language Model | Tokenizer | | |
|----------------------------------|---------------------------------|---|----------------------------------|----------------------------------|
| | | Stage 1 | Stage 2 | Stage 3 |
| LLM init | VideoGPT | - | - | - |
| Optimizer | AdamW | AdamW | AdamW | AdamW |
| Optimizer Hyperparameters | $\beta_1 = 0.9, \beta_2 = 0.96$ | $\beta_1 = 0.9, \beta_2 = 0.99, \epsilon = 1e^{-8}$ | $\beta_1 = 0.9, \beta_2 = 0.999$ | $\beta_1 = 0.9, \beta_2 = 0.999$ |
| Batch size per GPU | 4 | 32 | 8 | 12 |
| Peak learning rate | $1e^{-4}$ | $1e^{-4}$ | $1e^{-4}$ | $1e^{-4}$ |
| Discriminator peak learning rate | - | - | - | $1e^{-4}$ |
| Learning rate schedule | Cosine | Cosine | Cosine | Cosine |
| Training steps | 1000K | 1000K | 500K | 500K |
| Discriminator start steps | - | - | - | 20K |
| Warm-up steps | 10K | 10K | 10K | 10K |
| Weight decay | 0.03 | $1e^{-4}$ | $1e^{-4}$ | $1e^{-4}$ |
| Numerical precision | float16 | float16 | float16 | bfloat16 |

Table 9. The detailed training hyperparameters of SweetTokenizer.

separate validation and test sets for model evaluation. The dataset is widely used for researchs in computer vision.

6.3. Notations

The meaning of our notations appeared in the main paper are explained in Table 7.

6.4. Training Settings

The detailed training hyper-parameter settings for SweetTokenizer are reported in Table 9.

7. Additional Results

7.1. Generation results for ImageNet

Following the OmniTokenizer protocol [45], we train a VideoGPT-based generator on ImageNet-1K. As shown in Table 8, SweetTokenizer consistently outperforms all baselines in terms of FID. With fewer tokens, SweetTokenizer achieves 5.48 FID, outperforming OmniTokenizer by 26.4%. These results align with findings on UCF-101, reinforcing that fewer tokens lead to better generation performance.

7.2. More Visualizations

Fig 8 and Fig 7 visualize the reconstruction results for the UCF-101 and K-600 datasets. The pixel-level differences between ground truth and model are shown, with brighter areas indicating greater disparity and darker areas reflecting consistency. As shown, SweetTokenizer exhibits fewer reconstruction differences compared to OmniTokenizer, demonstrating its superior performance.

Fig 8 and Fig 9 visualize the reconstruction and generation results of SweetTokenizer on ImageNet-1K. For reconstruction, differences between models are highlighted in red blocks, with details shown in green blocks. Clearly, SweetTokenizer outperforms all baselines by a significant margin.

Finally, we visualize the words from our LLM codebook in Fig 10, based on few-shot video action recognition tasks

on the UCF-101 dataset. We use adjectives, nouns, adverbs, and verbs as prompts to Qwen LLM for action prediction. Green and orange indicate meaningful words, while red marks meaningless ones. The visualization shows that correct verb words consistently lead to accurate predictions, even when other words are irrelevant, highlighting the importance of our adverb and verb LLM codebook modules for video action recognition.

8. Limitations

Our tokenizer is not suitable for tasks requiring precise semantic understanding, like VQA, because the LLM codebook is trained in an unsupervised manner. Without additional constraints, such as contrastive learning between image features from Qwen-VLM and text embeddings in our codebook, aligning the image and text domains is challenging. A promising direction for future work is to enhance SweetTokenizer into a semantically strong tokenizer by contrastive learning.

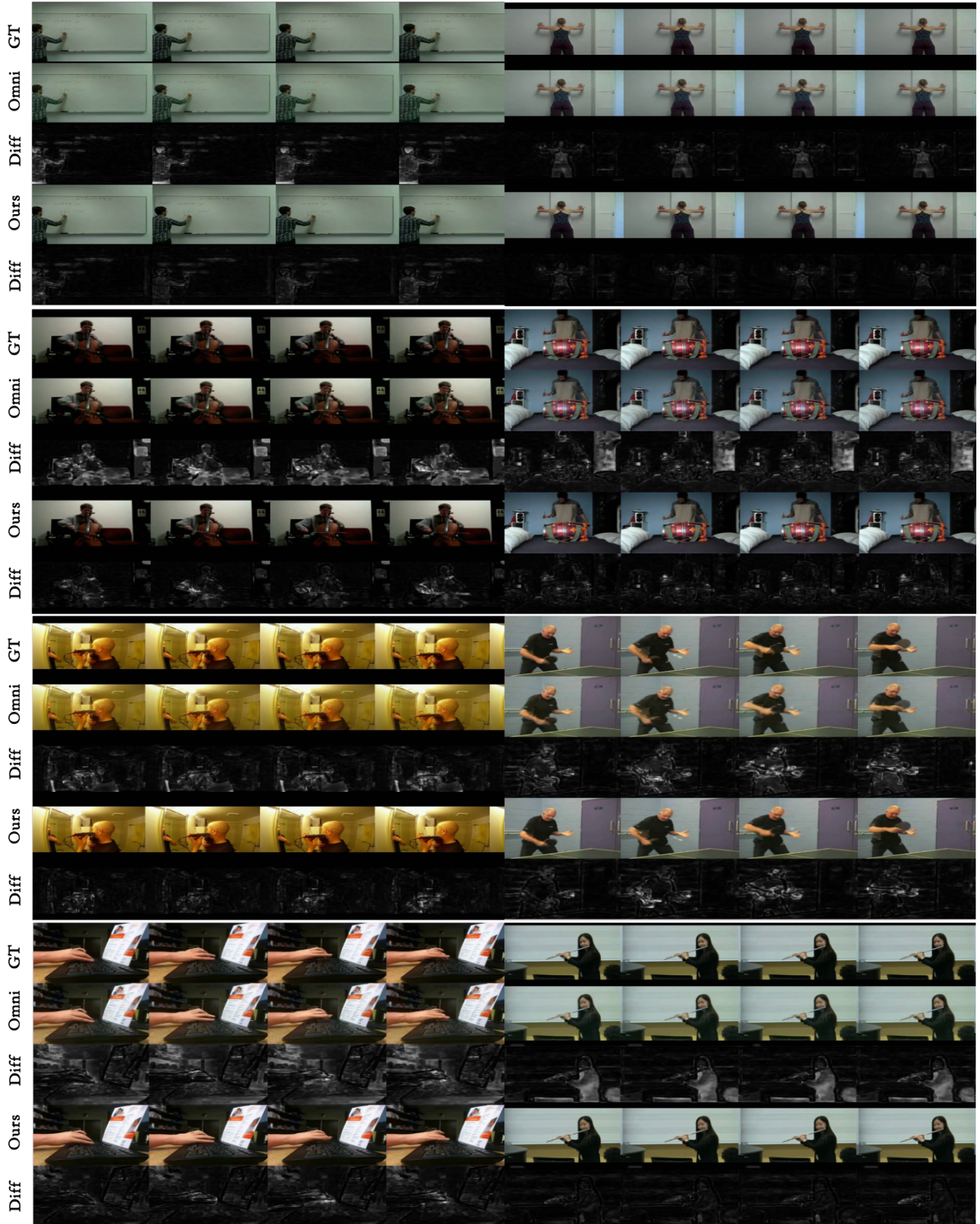


Figure 6. Comparison of the reconstruction results of OmniTokenizer and SweetTokenizer on UCF-101 dataset, where "Diff" represents the pixel difference between the ground truth and the models.

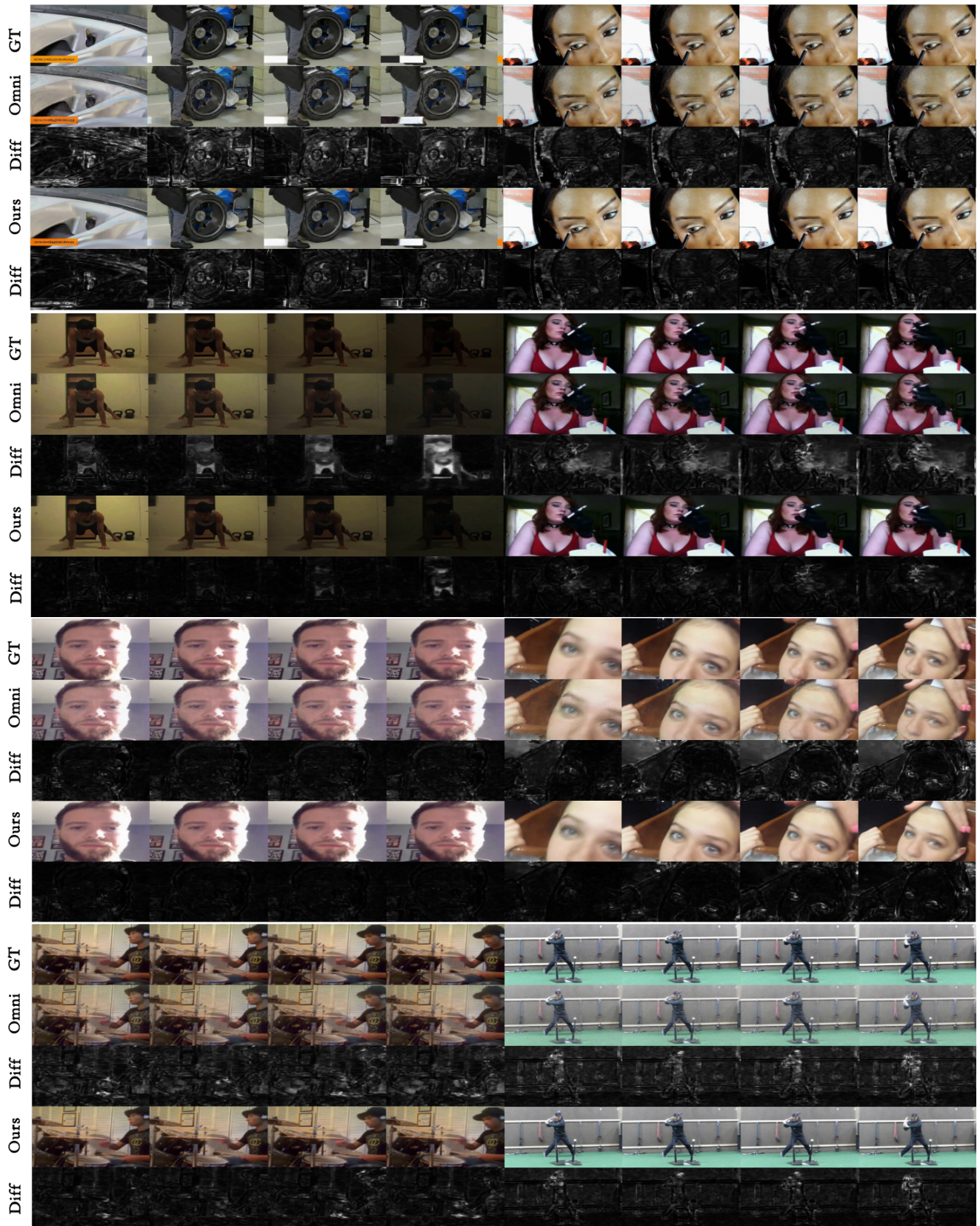


Figure 7. Comparison of the reconstruction results of OmniTokenizer and SweetTokenizer on K-600 dataset, where "Diff" represents the pixel difference between the ground truth and the models.

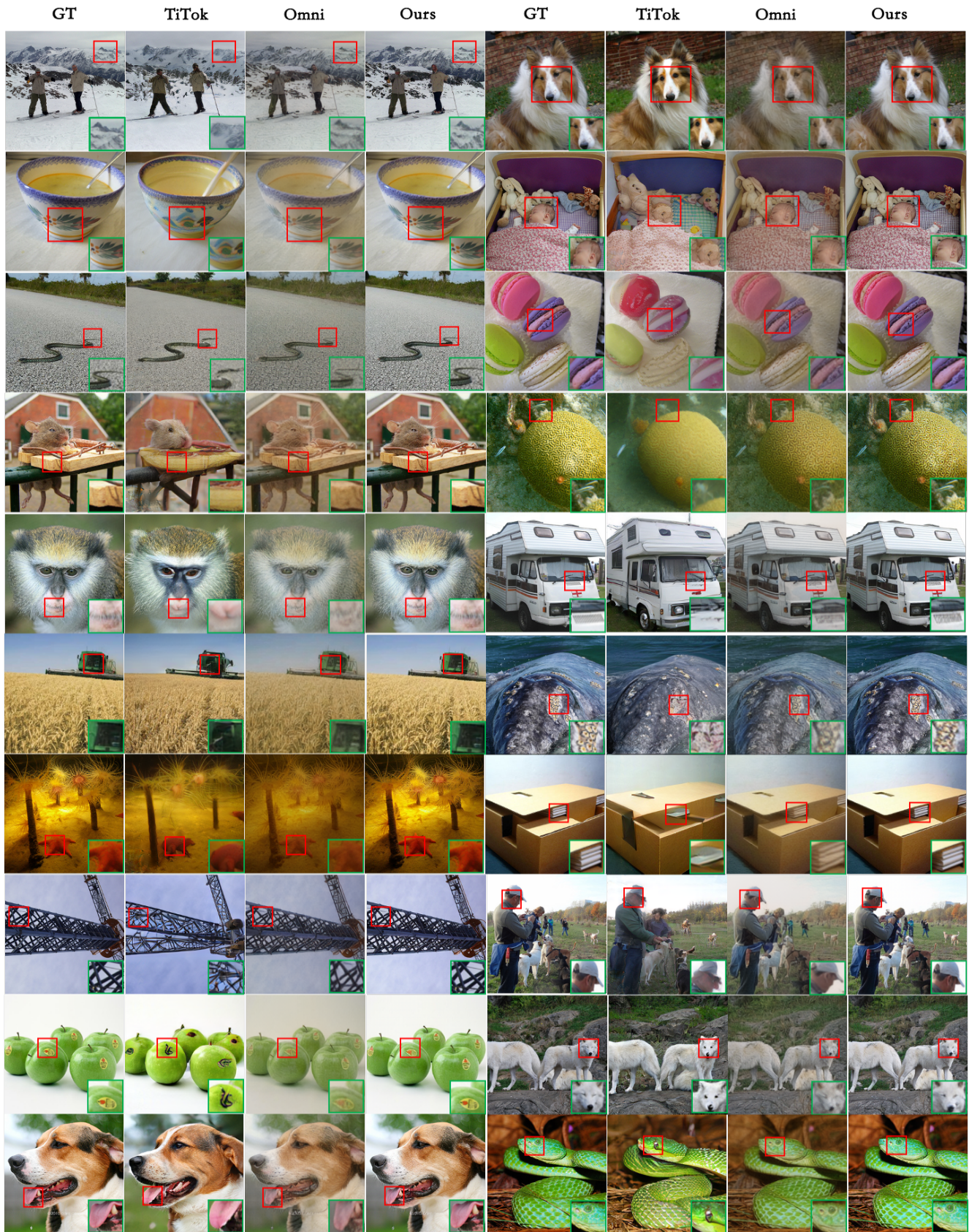


Figure 8. Comparison of the reconstruction results of TiTok, OmniTokenizer, and SweetTokenizer on ImageNet-1K dataset. Differences are selected by the red blocks and highlighted in the green blocks.



Figure 9. Class-conditional image generation results using SweetTokenizer, on ImageNet-1k dataset.

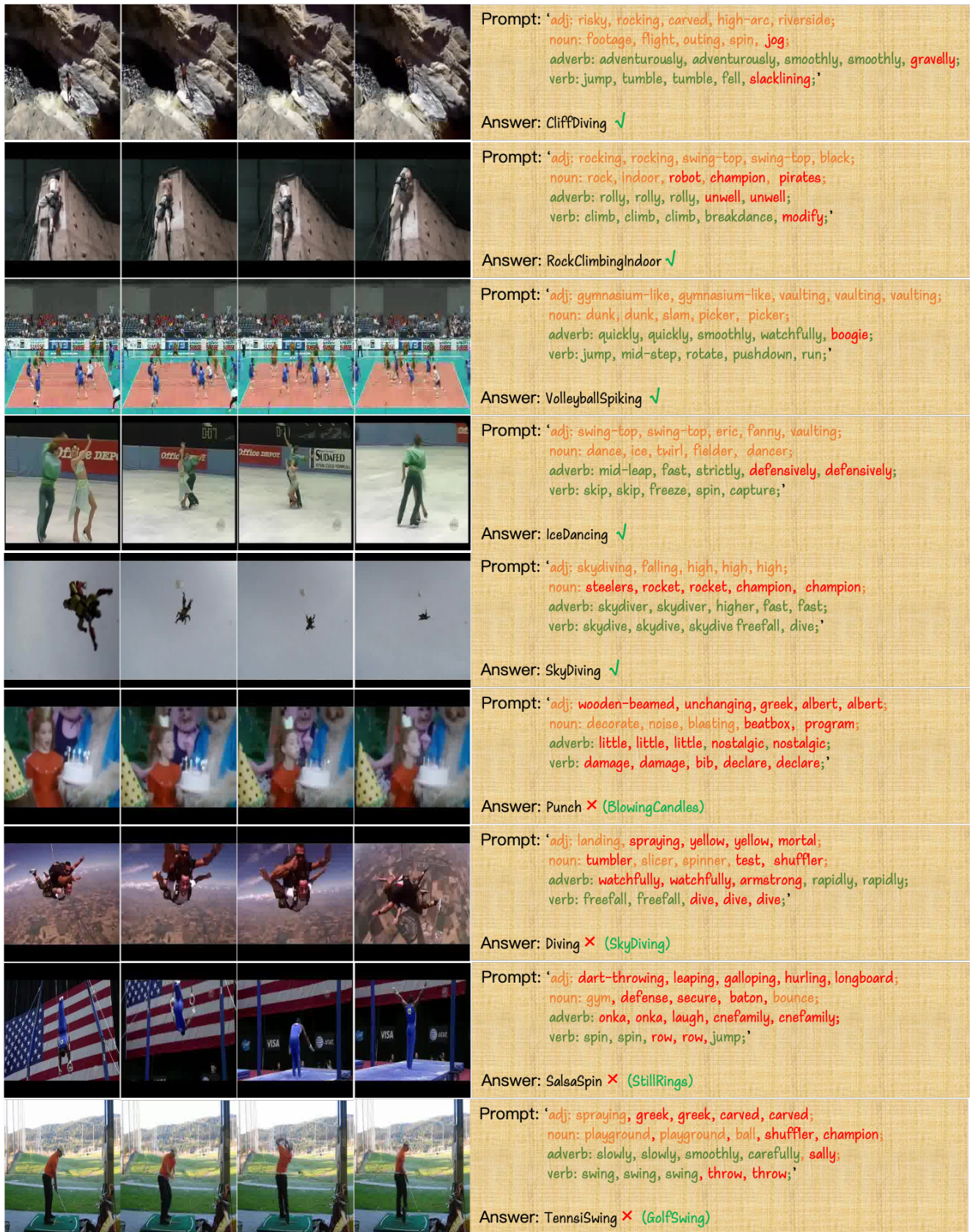


Figure 10. Semantic words visualization for UCF-101. The visualization is based on few shot video action recognition tasks.